Journal of Magnetic Resonance 243 (2014) 33–39

Contents lists available at ScienceDirect

Journal of Magnetic Resonance

journal homepage: www.elsevier.com/locate/jmr

2Q NMR of ^2H_2O ordering at solid interfaces

Tatiana V. Krivokhizhina, R.J. Wittebort *

Department of Chemistry, 2320 S. Brook St., University of Louisville, Louisville, KY 40208, USA

ARTICLE INFO

Article history:
Received 15 October 2013
Revised 7 February 2014
Available online 19 March 2014

Keywords:
Multiple-quantum spectroscopy
Double-quantum filtration
Pulse sequence
Phase cycle
Relaxation
Solvent ordering
Elastin
Collagen

ABSTRACT

Solvent ordering at an interface can be studied by multiple-quantum NMR. Quantitative studies of ^2H_2O ordering require clean double-quantum (2Q) filtration and an analysis of 2Q buildup curves that accounts for relaxation and, if randomly oriented samples are used, the distribution of residual couplings. A pulse sequence with absorption mode detection is extended for separating coherences by order and measuring relaxation times such as the 2Q filtered T_2. Coherence separation is used to verify 2Q filtration and the 2Q filtered T_2 is required to extract the coupling from the 2Q buildup curve when it is unresolved. With our analysis, the coupling extracted from the buildup curve in ^2H_2O hydrated collagen was equivalent to the resolved coupling measured in the usual 1D experiment and the 2Q to 1Q signal ratio was in accord with theory. Application to buildup curves from ^2H_2O hydrated elastin, which has an unresolved coupling, revealed a large increase in the 2Q signal upon mechanical stretch that is due to an increase in the ordered water fraction while changes in the residual coupling and T_2 are small.

1. Introduction

Solvent molecules interacting with a surface can be differentiated from the bulk solvent and studied using multiple-quantum (MQ) spectroscopy. The first examples were ^{131}Xe interacting with a glass surface [1] and strain induced ordering of ^2H_2O in blood vessels [2]. The key feature of this approach is that quadrupolar or dipolar couplings in the bulk, isotropic phase are averaged to zero while molecules at the surface are weakly ordered and have a non-zero coupling. The residual coupling is used to generate MQ coherence and the characteristic response of the MQ coherence to shifts in the transmitter offset or phase is used to separate or filter NMR signals from molecules at the surface. Herein we address practical aspects of this approach when applied to an important class of interfacial phenomena; water at the surface of a matrix protein. From an NMR perspective, water is an attractive probe since the anisotropic spin coupling can be dipolar (between protons) or quadrupolar (if the solvent is labeled with ^2H_2O or $H_2^{17}O$). In this paper, we discuss the simplest case, ^2H NMR, which has a single double-quantum (2Q) transition. Applications have included the observation of ordered water in elastin [3], purple membrane [4] and tendon [5–7] and likely involve water interacting at the nonpolar surface of a hydrophobic protein or at the polar surface of a hydrophilic protein.

Important properties to be determined are the degree of solvent ordering and the solvent accessible surface area. These are closely related to two NMR parameters, the residual quadrupole coupling and the intensity of the indirectly detected 2Q signal. In this paper we address practical difficulties that arise when these parameters are measured. The goals are to confirm adequate 2Q filtration and to develop a quantitative analysis of 2Q buildup data that incorporates relaxation and the distribution of residual couplings inherent to randomly oriented samples. In many cases, the coupling is not resolved [1,3,8] so detection of an antiphase doublet using the standard sequence can lead to signal cancellation. Also, overlap of a potentially large signal from the bulk solvent occurs if 2Q filtration is insufficient. To eliminate cancellation of antiphase signals, absorption mode signals are detected [7,9] and, to confirm that 2Q filtration is adequate, we have added a constant time indirect dimension for separating coherences by order. The sequence with absorption mode detection is also extended so that three relaxation times specific to the ordered solvent, T_1 and T_2 with 2Q filtration and $T_{2,2Q}$, can be measured. With randomly oriented samples, there is a "powder" distribution of quadrupole coupling frequencies and this is incorporated into our analysis. The pulse sequence and analysis are tested against collagen and applied to elastin. Collagen has a small but resolved quadrupolar coupling and we show that this coupling can be determined from the buildup curve using our analysis albeit with less accuracy than measured in the 1Q experiment. Also, the observed 2Q signal strength is in accord with theory if relaxation and the powder distribution of couplings are accounted for. With elastin, the residual coupling is not

* Corresponding author.
E-mail address: dick.wittebort@louisville.edu (R.J. Wittebort).

http://dx.doi.org/10.1016/j.jmr.2014.02.022
1090-7807/

resolved and the detected NMR signal has a contribution from bulk solvent if 2Q filtration is not complete. With a purge period and a 64-step phase cycle, adequate filtration is confirmed by 2D separation of the coherences and we find that the residual quadrupole coupling and the mole fraction of ordered solvent can be determined from the buildup curve if T_2 of the ordered solvent is also measured. When elastin is subjected to mechanical strain, large changes in the 2Q spectra are observed and these are parsed into changes in the mole fraction of ordered solvent and the residual coupling.

2. Theory

The pulse sequence begins with the density operator at thermal equilibrium, i.e., aside from an invariant identity term and the Curie proportionality constant, $\rho_{eq} = I_z$. Standard density matrix theory with equation of motion $\dot{\rho} = -i[H, \rho]$ is used and implemented with scripts listed in the Appendix A.3. With rotating frame Hamiltonian, H, the density operator evolves according to

$$\rho' = U^{-1}\rho U \text{ with } U = e^{iHt}. \tag{1}$$

Quadrupole coupling, frequency offset and relaxation are reasonably neglected during pulses and the relevant Hamiltonian is

$$H_{RF} = \omega_1(\cos\phi I_x + \sin\phi I_y). \tag{2}$$

In the above, ω_1 is the resonant RF field strength and ϕ is the RF phase.

Pulse sequence design is facilitated by expanding ρ in operators related to coherences and populations of the spin system transitions. Here, we use the spin-1 single transition coherences of Wokaun and Ernst [10] combined with I_z and $Q = (3I_z^2 - 2)$ to represent the two independent populations (0Q coherences) [11]. This set is complete, trace orthogonal and expectation values are directly related to matrix elements of ρ by,

$$I_x^{(rs)} = \rho_{rs} + \rho_{sr}, \quad I_y^{(rs)} = i(\rho_{sr} - \rho_{rs}), \quad I_z = \rho_{11} - \rho_{-1-1} \text{ and}$$
$$Q = (\rho_{11} - 2\rho_{00} + \rho_{-1-1}). \tag{3}$$

Between pulses, coherent evolution is due to the quadrupole, H_Q, and offset, H_{OS}, Hamiltonians,

$$H = H_Q + H_{OS} = \omega_Q\left(I_z^2 - 2/3\right) - \omega_{OS}I_z, \tag{4}$$

where ω_Q and ω_{OS} are the effective quadrupole coupling and the offset frequencies. Relaxation and potentially spin exchange must also be accounted for when ω_Q is comparable to $1/T_2$. In the context of spin-3/2 ^{131}Xe NMR, Deschamps et al. [12] used an effective Liouvillian approach. With ^{2}H, the exchange narrowed limit can likely be assumed since the quadrupole coupling is small and narrow lines or well-resolved couplings are typically observed. In this limit, coherences relax with a single exponential time constant [13] and the effective quadrupole coupling is a population weighted average [14]. This assumption greatly simplifies subsequent calculations and a straightforward calculation shows that between pulses,

$$\rho_{rs}(t) = \rho_{rs}(0)\exp[-(i\bar{\omega}_{rs} + R^{(rs)})t] \text{ and}$$
$$I_z(t) = I_z + (I_z(0) - I_z)e^{-R_1 t} \approx I_z(0), \tag{5a}$$

with

$$\omega_{-10} = (\omega_{OS} + \omega_Q), \quad \omega_{01} = (\omega_{OS} - \omega_Q),$$
$$\omega_{-11} = 2\omega_{OS} \text{ and } \omega_{rr} = 0. \tag{5b}$$

In the above, $R^{(rs)}$ are reciprocal relaxation times and we have noted that longitudinal relaxation can be neglected when T_1 is long compared to the pulse sequence duration.

The sequence used here, Fig. 1, is a modification of sequences used previously for MQ NMR in isotropic solutions [9] and ^{1}H MQ NMR in tendon [6,7,15]. Unlike solution experiments, the coupling is not isotropic and the powder distribution of couplings in unoriented materials must be taken into consideration. The sequence, Fig. 1, has two indirect dimensions, either of which is typically held constant in a 2D experiment. The t_1 (preparation) dimension is used to determine the residual coupling when it is not resolved in the usual 1D experiment and coherences are separated by order in the t_2 (evolution) dimension. Unwanted coherences decay during τ' for absorption mode detection and transmitter phases, α, β and γ, are cycled for 2Q filtration. By varying τ or τ', $R_{2,2Q}$ or R_1 with 2Q filtration are determined and, with an optional refocusing pulse (dotted line), the 2Q filtered R_2 can be measured.

A flowchart summarizing the density operator at the end of each period through conversion is shown in Fig. 2. Expressions for the coherence transfers were obtained by numerical simulations of Eqs. (1)-(5) (see Appendix A.3). During preparation, I_z is partially transformed into 2Q coherence [16,17]. With $\alpha = 0°$, the initial 90° pulse converts I_z into in-phase 1Q coherence $\left(\sqrt{2}\left(I_y^{-10} + I_y^{01}\right)\right)$. Subsequently, the 1Q transitions rotate at frequencies $\omega_{OS} \pm \omega_Q$ and relax with rate R_2. At the end of preparation, net evolution from the frequency offset is eliminated by the central 180° pulse and the 2nd 90° pulse converts in-phase and anti-phase $\left(\sqrt{2}\left(I_y^{-10} - I_y^{01}\right)\right)$ 1Q coherences into 0Q (I_z) and 2Q $\left(I_y^{-11}\right)$ coherences, respectively [17,18]. Bulk solvent ($\omega_Q = 0$) present in the sample adds to the 0Q coherence and the effect of non-ideal pulse widths is to add 1Q coherence.

Coherences created during preparation are separated by order in t_2 and we use this to determine if 2Q filtration is adequate. Ideally, the detected NMR signal is only from the 2Q coherence prepared from the ordered solvent. Losses from relaxation during this period are negligible if the duration, τ, is small compared to $T_{2,2Q}$ and this is achieved by using an offset frequency that is large compared to $R_{2,2Q}$ and sampling a small number of t_2 values at a frequency harmonically related to the offset (see below). An alternative method for separating coherences is to advance the transmitter phase [19]. However, this method and 2Q filtration place similar demands on phase shift accuracy and this is avoided here.

For absorption mode detection, 2Q coherence is converted to and stored as I_z [7,9] and then, after a delay τ', converted to observable 1Q coherence by the final 90° pulse. During τ', unwanted coherences are allowed to decay. In practice, $\tau' \sim 3T_2$ is satisfactory and shorter τ' could be used if gradients are applied. Unwanted signal from I_z terms generated during preparation (the bottom path in Fig. 2) and from bulk solvent are eliminated by the phase cycle described in the Appendix A.1.

With a phase cycle that adds signals coherently along the "2Q path" and cancels signals from other paths, the NMR signal at the beginning of detection is (R_1 relaxation neglected),

$$S(t_1, t_2) = e^{-2R_2t_1 - R_{2,2Q}\tau}\cos(2\omega_{OS}t_2)\int \sin^2(\omega_Q(\Omega)t_1)d\Omega. \tag{6}$$

The exponential factor accounts for relaxation in the course of the pulse sequence and the integral indicates a powder average over orientations of the coupling tensor. With the assumption of axially symmetric coupling, $\omega_Q = \omega_{||}(3\cos^2\theta - 1)/2$, and the substitution, $x = \cos\theta$, the above simplifies as follows for the preparation experiment ($\tau = t_2 = 0$):

$$S(t_1) = S_{\text{prep}}\, e^{-2R_2t_1}\int_0^1 \sin^2\left[\frac{\omega_{||}}{2}(3x^2 - 1)t_1\right]dx. \tag{7}$$

In Eq. (7), $\omega_{||}$ is the quadrupole coupling constant and a constant, S_{prep}, was inserted to account for the gain of the NMR instrument.

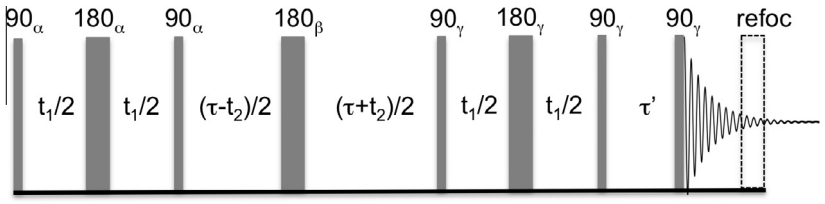

Fig. 1. Sequence for 2Q spectroscopy with symmetric preparation/conversion and constant time evolution. RF pulse phases are α, β and γ as indicated.

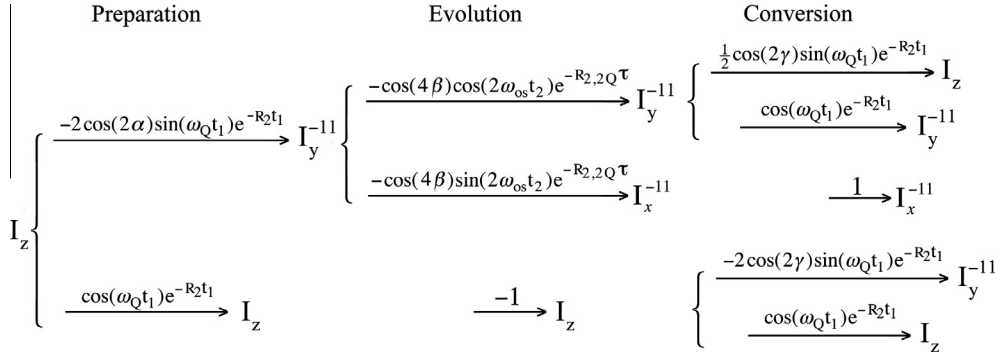

Fig. 2. Density operator flowchart for the indicated periods of the pulse sequence, Fig. 1. For 2Q filtration, the upper "2Q path" is selected. Functions above the arrows are stepwise transfer efficiencies and the net transfer along a path is the product of these functions. The phase factors are for integral multiples of 90° (α and γ) or integral multiples of 45° (β). With α and γ constrained in this way, I_y^{-11} and not I_x^{-11} is prepared from and converted to I_z [16].

With standard identities ($\sin^2\theta = (1-\cos 2\theta)/2$ and $\cos(\xi-\psi) = \cos\xi\cos\psi + \sin\xi\sin\psi$), Eq. (7) is expressed in a convenient form for numerical evaluation,

$$S(t_1) = \frac{1}{2} S_{prep}\, e^{-2R_2 t_1}\{1 - u^{-1}[C(u)\cos\omega_{\|} t_1 + S(u)\sin\omega_{\|} t_1]\}, \quad (8a)$$

with

$$u = (3\omega_{\|} t_1)^{1/2}, \quad C(u) = \int_0^u \cos x^2\, dx \text{ and}$$
$$S(u) = \int_0^u \sin x^2\, dx. \quad (8b)$$

Relaxation neglected, the buildup curve rises to a maximum value in a time $t_1 \sim 1/(2\nu_{\|})$ and settles with damped oscillation to a constant value, $S_{prep}/2$, i.e., half the signal from a Bloch decay, S_{Bloch}, also initiated from spin equilibrium. This is different from either the 2Q solution NMR experiment or if the powder average is neglected wherein $S(t_1)$ oscillates at the coupling frequency.

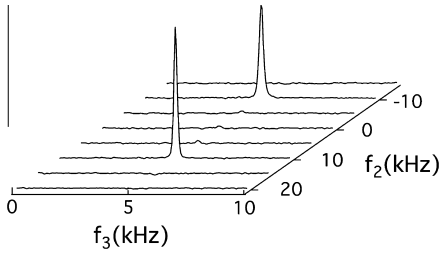

Fig. 3. 2D 2Q filtered spectrum of a relaxed elastin fiber hydrated with ^2H_2O obtained with a frequency offset of 5 kHz. The desired signal from 2Q coherence is at $f_2 = \pm 10$ kHz and unwanted signals not removed by the phase cycle or the purge (τ') would appear at $f_2 = 0$ or ±5 kHz.

3. Results

In Fig. 3, the efficiency of 2Q filtration was tested on a sample, unstretched bovine elastin, by separating coherences in f_2. This sample is a demanding test since it has a large fraction of unordered solvent (see below) and the ordered solvent residual coupling is unresolved. While phase cycles for 2Q filtration are readily devised with simulations, common experimental artifacts like RF inhomogeneity and errors in pulse phases and width are difficult to model and an experimental test is appropriate.

Complete 2Q filtration in the spectrum, Fig. 3, was obtained with the combination of a 10 ms purge, τ', and a 64-step phase cycle. With a 5 kHz offset, signals from 2Q coherence are observed at $f_2 = \pm 10$ kHz and signals from the bulk solvent (0Q) or from imperfect pulses (1Q) at 0 and ±5 kHz are below the noise level. Transmitter phases were cycled as follows: $\alpha = 4\times 0°$, $4\times 90°$, $4\times 180°\ldots$, $\beta = 16\times 45°$, $16\times 135°$, $16\times 225°\ldots$, and $\gamma = 0°$, 90°, 180°… with receiver phase: 0°, 270°, 180°, 90°, 180°, 90°, 0°, 270°, where $4\times 0°$ indicates that 0° is repeated 4 times. The 2D spectrum was acquired with eight t_2 increments sampled at $8\nu_{OS}$. Since the length of the evolution period, $\tau = 175$ μs, is short compared to $T_{2,2Q} \sim 5$ ms, losses due to relaxation are negligible. With complex Fourier transformation in t_2, 2Q signals are at $+2\nu_{OS}$ and $-2\nu_{OS}$ because only I_y^{-11} and not I_x^{-11} is converted, Fig. 2.

The reliability (i) that the quadrupole coupling can be recovered from a buildup experiment and (ii) that the 2Q signal intensity is accounted for by Eq. (8) were tested by directly determining the quadrupole coupling and T_2 in a sample with a small resolved coupling, Fig. 4a and b, and comparing these to the values determined by least squares fitting of the buildup curve to Eq. (8), Fig. 4c and d. The ^2H spectrum of collagen hydrated with ^2H_2O has a small axially symmetric coupling of 1.95 kHz, Fig. 4a, and a central feature likely due to water on the surface of the sample and sample tube.

The central feature is removed in the 2Q filtered powder pattern, Fig. 4a dotted line, discussed below. T_2 and ν_Q determined by a χ^2 (least squares) fit of Eq. (8) to the 2Q buildup data are listed

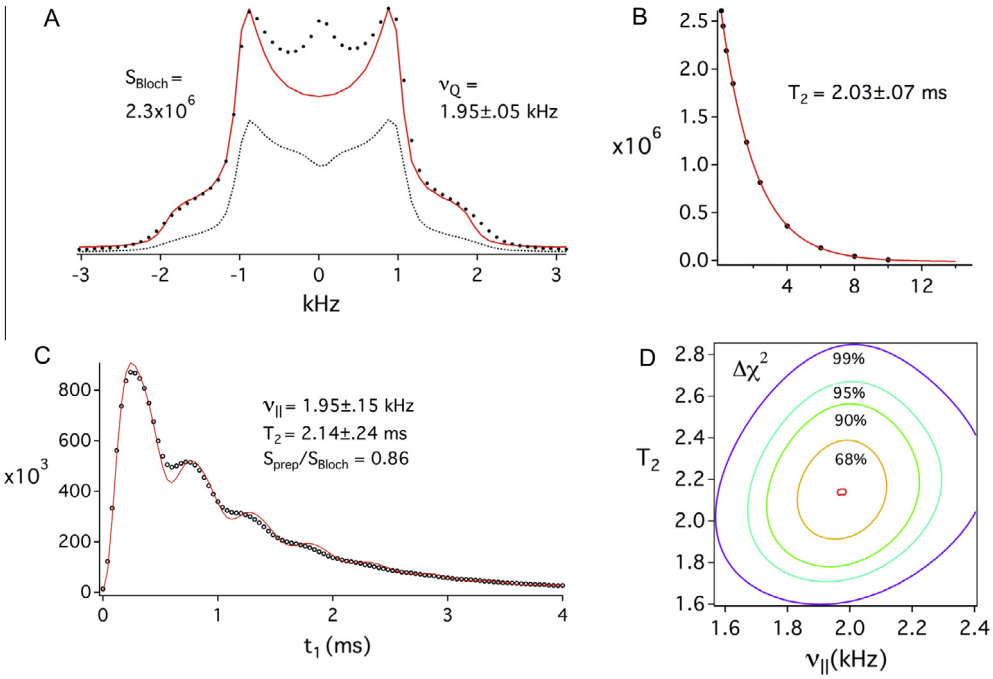

Fig. 4. (a) Bloch decay (circles), simulated (red line) and 2Q filtered (dotted) ^{2}H spectra of randomly oriented, hydrated collagen. (b) Spectrum integral (circles) as a function of solid echo delay, τ, and single exponential fit (red) with the indicated T_2. (c) Buildup curve (open circles) and χ^2 (least squares) fit to Eq. (8) (red line). (d) Contour plot of $\Delta\chi^2 = (\chi^2 - \chi^2_{min})/\chi^2_{min}$. Indicated uncertainties are from the 68% confidence contour, $\Delta\chi^2 = 1$ [20]. (For interpretation of the references to color in this figure legend, the reader is referred to the web version of this article.)

in Fig. 4c. The fit shows a well-defined χ^2 minimum, Fig. 4d, at the same coupling and T_2 observed in the usual 1D spectra, Fig. 4a and b, albeit with less accuracy. Error limits at the 68% confidence level were obtained from the $\Delta\chi^2 = 1$ contour [20], Fig. 4d.

Oscillations in the buildup curve, Fig. 4c, are observed only when the coupling is resolved, in which case 2D Fourier transformation of the data table provides a useful result: the $f_1 = 0$ slice is a good representation of the 2Q filtered powder pattern, Fig. 4a (dotted line). The small dip in the center of the pattern can be attributed to the fact that 2Q coherence is only excited for nonzero quadrupole coupling. Aside from a method for broadband excitation of 2Q coherence [21], this result is difficult to obtain and it is shown in the Appendix A.2 how this follows from Eq. (6).

Insofar as the pulse sequence works as described and the sample contains only water with a non-zero coupling, then the signal intensity, S_{prep}, determined from the buildup curve and that from a Bloch decay, S_{Bloch}, are equal. In the example above, S_{prep} is 86% of S_{Bloch} and the difference can be attributed to the small amount of unordered water in the hydrated collagen sample, imperfections in the pulse sequence and T_1 relaxation during τ'. Note that spectra in Fig. 4 were obtained without a resonance offset so the three 180° refocusing pulses were eliminated. Restoring these, one at a time, systematically decreased the signal intensity by a nearly constant stepwise factor of ~0.92. In general, efficiency of the refocusing pulses will depend on strength and homogeneity of the RF field over the sample under study.

Buildup curves for a ^2H_2O hydrated elastic fiber of bovine elastin, relaxed and stretched to 150% of its relaxed length, are shown in Fig. 5a. In these examples, the residual quadrupole coupling is unresolved and we find that buildup data alone do not yield unique values of T_2 and ν_Q. Consequently, 2Q filtered T_2's, were independently measured (Fig. 5b and c, lower traces). Over the time scale of the preparation experiment, 15 ms, T_2 relaxation is well described by a single exponential justifying the use of Eq. (8). With T_2 constrained in this way, fits of Eq. (8) to the buildup data yield the unique ν_Q and S_{prep} parameters summarized in Fig. 5a. The buildup data and S_{prep} values are normalized relative to the bulk NMR signal obtained with a Hahn echo extrapolated to zero echo delay (Fig. 5b and c, upper traces). Spectrometer artifacts aside, this is equivalent to the Bloch decay signal and the "bulk" T_2 provides an additional NMR parameter.

While elastin solvent T_2 values are significantly shorter than we measured in pure ^2H_2O (6–7 ms compared to ~200 ms), the effect of stretching the fiber on these relaxation times is small and comparable to experimental uncertainties. By contrast, there is an order of magnitude increase in the intensity of the buildup curve when the fiber is stretched. Parsing the change into the two parameters, ν_Q and S_{prep}, shows an order of magnitude increase in S_{prep}, the fraction of ordered water in the sample, while the change in the residual coupling is small.

4. Discussion

The focus of this paper is ^{2}H MQ NMR of solvent water (^2H_2O) interacting with a protein matrix. In many applications, the residual quadrupole coupling of solvent localized at a surface is small and not resolved. To avoid signal cancellation that occurs when an unresolved, antiphase doublet is detected, we use a sequence with absorption mode detection [7,9]. The sequence is modified so that coherences can be separated by order and relaxation times with 2Q filtration can be measured. Clean silencing of signals from the bulk solvent and pulse imperfections is confirmed by 2D separation of coherences, Fig. 3.

Important properties to be determined in water/protein systems are the mole fraction of water in the sample that is ordered at the protein surface and the solvent residual coupling. To determine these from 2Q buildup experiments, our analysis incorporates spin relaxation and the powder distribution of quadrupole couplings inherent to randomly oriented samples. The analysis

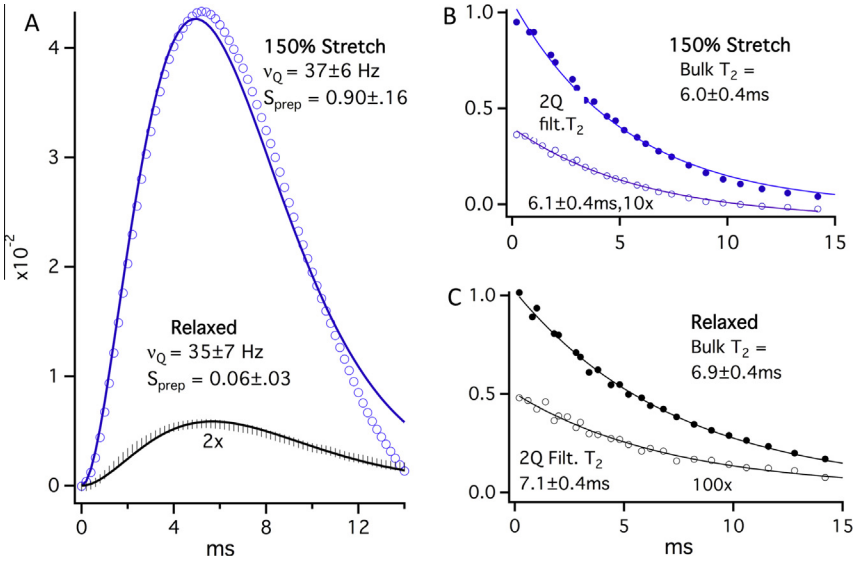

Fig. 5. ^2H_2O 2Q buildup curves (a) and T_2 values (b and c) for stretched (blue) and relaxed (black) elastin. Signal intensities are normalized relative to the exponential fits of the "bulk" T_2 data extrapolated to zero echo delay. Vertical scales of the 2Q filtered T_2 data (open circles, b and c) and the buildup curve for relaxed elastin (black, a) were expanded as indicated. (For interpretation of the references to color in this figure legend, the reader is referred to the web version of this article.)

was tested with two ^2H_2O hydrated samples: collagen which has a small but resolved solvent coupling and elastin that has an unresolved solvent coupling. In the former, analysis of the 2Q buildup curve from the 2D preparation experiment yielded the same residual coupling and T_2 that were determined by the usual 1D methods. Moreover, the ratio of 2Q to 1Q signal intensities was in accord with the analysis indicating that the fraction of ordered solvent in the system can also be estimated from the 2Q buildup curve. We also find that an undistorted 2Q filtered powder pattern is obtained from the 2D Fourier transform of the preparation experiment. With hydrated elastin, it was necessary to separately measure T_2 of the ordered solvent, ^2H_2O, to determine a unique value for the coupling constant from the buildup curve. By stretching the sample, we find that the 2Q buildup curve is a sensitive measure of the effect of mechanical strain on the solvent component of the elastomer and that this can be parsed into changes in the ordered solvent fraction and the residual coupling. A more complete set of experimental data and analysis of stretch induced solvent ordering and its relation to elastic recoil will be presented elsewhere.

5. Materials and methods

The ^2H_2O hydrated collagen sample was obtained from a Sprague-Daley rat. Tails excised from euthanized animals were stored at −4 °C for later use. After thawing, collagen fibers were pulled from a tail and exchanged overnight in ^2H_2O. After blotting on filter paper to remove surface moisture, 34 mg of fibers were transferred to a short (1.5 cm) 3 mm NMR tube for vapor phase equilibration against ^2H_2O in a closed vessel for 24 h. at 40 °C after which the fiber mass decreased by 10%. Immediately after removal from the equilibration chamber, the tube was sealed with epoxy glue. Fibers prepared in this way retain native-like flexibility.

Bovine elastin fibers, prepared by the neutral extraction method [22], were obtained from Elastin Products Company (Owensville, MO, 65066). An ~10 mg fiber, ~1 mm × 10 mm, was glued to short 1/16″ diameter G10 rods (length ~1 cm). The fiber was equilibrated against solvent to a known mass and inserted into a 3 mm NMR tube (length ~2 cm). The tube was sealed and the rods held in place with parafilm. The fiber was stretched to a measured length by moving the rods and again securing their positions with parafilm.

NMR spectra were obtained on an 11.7 T instrument with a Libra data system (Tecmag, Houston TX,) and homebuilt RF electronics. The probe is based on a design previously described [23]. With 150 watts RF power at the ^2H frequency, 76.05 MHz, the 90° pulse width was 2.5 μs. T_2 relaxation times were measured with 90° (collagen) or 180° (elastin) refocusing pulses inserted after a 90° pulse (to measure the bulk T_2) or the sequence in Fig. 1 (to measure the 2Q filtered T_2). While the 180° pulse used in the elastin experiments refocuses the frequency offset, 5 kHz, but not the much smaller quadrupole splitting, ~20 Hz, simulations show that the resulting error in T_2 is comparable to the error limits indicated in Fig. 5.

Appendix A

A.1. Phase cycle for 2Q filtration

Using Fig. 2, the overall phase dependence of the density operator terms along the 2Q path, ρ, and the 1Q path, ρ', are

$$\rho \propto \cos(2\alpha)\cos(4\beta)\cos(2\gamma)(\cos\gamma I_x - \sin\gamma I_y) \text{ and}$$
$$\rho' \propto -(\cos\gamma I_x - \sin\gamma I_y) \quad \text{(a1)}$$

Preparation and conversion phases, α and γ, are limited to integral multiples of 90° and the 2Q refocusing phase, β, to odd integral multiples of 45°. The last factor in ρ and ρ' is from the transformation of I_z by the final 90° pulse of the sequence, Fig. 1.

$$I_z \xrightarrow{(90)_x} \cos\gamma I_y - \sin\gamma I_x. \quad \text{(a2)}$$

The convention for γ in Eq. (a2) is the same as Eq. (2) for H_{RF}, i.e., advancing the phase is an anticlockwise rotation in the rotating frame and a 90° pulse with phases 0°, 90°, 180°, 270° transforms I_z to I_y, $-I_x$, $-I_y$, I_x, respectively. The phase factors for preparation and conversion, $\cos(2\alpha)$ and $\cos(2\gamma)$, result from the change in coherence order, ±2 [19]. The factor $\cos(4\beta)$ in Eq. (a1) for ρ is the 2Q analog of the well-known fact that a 90° rotation of the refocusing pulse phase in a Hahn (1Q) echo shifts the echo phase by 180°.

Direct substitution of the 64-step cycle from Fig. 2 into eq.'s a1 yields an 8-step repeat for ρ and a 4-step repeat for ρ':

$$\rho \propto -I_y, -I_x, I_y, I_x, I_y, I_x - I_y, -I_x \text{ and } \rho' \propto -I_y, I_x, I_y, -I_y. \quad \text{(a3)}$$

Note that in the first and last 4 steps, rotation of ρ is in the opposite sense indicated by Eq. (a2) and for ρ'. Thus, with the 8-step receiver cycle, 0°, 270°, 180°, 90°, 180°, 90°, 0°, 270°, signals from the 2Q path, ρ, add and signals from the unwanted 1Q path, ρ', cancel. Straightforward calculation shows that coherences along the other paths in Fig. 2 also cancel.

A.2. 2Q filtered powder pattern

With the phase cycle described above, the free induction signal in the 2Q filtered preparation experiment, i.e., the signal from the upper path in Fig. 2, is

$$S(t_1, t_3) = S_{prep} \sin^2[\omega_Q(\Omega)t_1]e^{-2R_2t_1} \cos[\omega_Q(\Omega)t_3]e^{-R_2t_3}. \quad \text{(a4)}$$

With standard identities, $\sin^2 x = (1 - \cos 2x)/2$ and $\cos x = (e^{ix} + e^{-ix})/2$, Eq. (a4) is rewritten as follows:

$$S(t_1,t_3) = \frac{1}{4}S_{\text{prep}}\left[1 - (e^{2i\omega_Q(\Omega)t_3} + e^{-2i\omega_Q(\Omega)t_3})/2\right]e^{-2R_2t_1}\left(e^{i\omega_Q(\Omega)t_3} + e^{-i\omega_Q(\Omega)t_3}\right)e^{-R_2t_3}. \quad \text{(a5)}$$

With the relation

$$g(\omega \pm \omega_Q) \equiv \int_0^\infty e^{-[i(\omega\pm\omega_Q)+R_2]t}\,dt = [i(\omega \pm \omega_Q) + R_2]^{-1}, \quad \text{(a6)}$$

Fourier transformation of Eq. (a5) with respect to t_1 and t_3 is

$$S(\omega_1, \omega_3) = \frac{1}{4}S_{\text{prep}}\{g(\omega_1) - [g(\omega_1 + 2\omega_Q) + g(\omega_1 - 2\omega_Q)]/2\}\{g(\omega_3 + \omega_Q) + g(\omega_3 - \omega_Q)\}. \quad \text{(a7)}$$

For a well-resolved doublet, $g(\omega_1 \pm 2\omega_Q) \approx 0$ when $\omega_1 = 0$ and we obtain

$$S(0, \omega_3) \approx \frac{1}{4}S_{\text{prep}}R_2^{-1}[g(\omega_3 + \omega_Q) + g(\omega_3 - \omega_Q)]. \quad \text{(a8)}$$

Integrated over powder orientations, Ω, Eq. (a8) yields the usual Pake doublet with signal intensity proportional to T_2.

A.3. Octave scripts

Representative octave scripts that have been used are listed below. The script **dq_prepare.m** calculates evolution of the density operator in the preparation sequence, (90–t_1/2-180–t_1/2-90). Calls to, **ops3levels.m**, **evol_ThPh.m**, **evol_1_Q_CS.m** and **decomp_1.m** calculate, respectively, matrix representations of the operators, RF pulse transformations, evolution during delays, and decomposition of the density matrix into basis operators. The script **prepCurve.m** calculates a preparation curve according to Eq. (8) using a library function quadgk for the numerical integrations.

dq_prepare.m

```
# Set the quad. coupling, vq, and offset, vos (Hz).
  vq=1
  vos=0
# Initialize sequence by creating relevant operators
  ops3levels;
# set the initial density operator to Iz
  rho=Iz;
# step 1: 90° x-pulse
  Th=90;
  Ph=0;
  evol_ThPh;
# step 2: delay for time t_evol (s)
  t_evol=1/8
  evol_1_Q_CS;
# step 3: 180° x-pulse
  Th=180;
  Ph=0;
  evol_ThPh;
# step 4: delay for time t_evol
  t_evol=1/8;
  evol_1_Q_CS;
# step 5: 90° x-pulse
  Th=90;
  Ph=0;
  evol_ThPh;
# decompose rho into single transition operators and print to
  screen
  decomp_1;
  real(st)
```

ops3levels.m

```
# Prepares the 6 3x3 matrix representations of I = 1 single
  transition
# coherences, Ix(r,s)=I(1,r,s,:,:) and Iy(2,r,s,:,:); r=1->2, s=r+1-
  >3,
# 2 orthogonal polarization operators (Iz,Q), Ix, Iy and the
  raising operator, Ip
  dum=zeros(3);
  for r=1:1:2;
    for s=r+1:1:3;
      I(1,r,s,:,:)=dum(:,:);
      I(1,r,s,r,s)=1/2;
      I(1,r,s,s,r)=1/2;
      I(2,r,s,:,:)=dum(:,:);
      I(2,r,s,r,s)=-i/2;
      I(2,r,s,s,r)=i/2;
    endfor;
  endfor;
# Iz
  j=1;
  Iz=diag([j:-1:-j]);
# Q=quadrupolar order=Iz*Iz-I(I+1)
  Q=3*(Iz*Iz)-2*eye(3);
# Ix
  Ix=zeros(2*j+1);
  n=1;
  while (n<2*j+1)
    Ix(n,n+1)=0.5*sqrt(n*(2*j+1-n));
    Ix(n+1,n)=0.5*sqrt(n*(2*j+1-n));
    n++;
  endwhile
#Iy: Iz and Ix are defined, so we use [Iz,Ix]=iIy to find Iy
  Iy=(1/i)*(Iz*Ix-Ix*Iz);
  Ip=Ix+i*Iy;
```

evol_ThPh.m

```
# evolution of the current density operator, rho, subject to a
  hard RF
# pulse with flip angle Th (deg) and phase Ph (deg)
  phir=pi*Ph/180;
  thetar=pi*Th/180;
  op=(cos(phir)*Ix)+(sin(phir)*Iy);
  prop=expm(-i*(thetar)*op);
  r=prop'*rho*prop;
  rho=r;
```

evol_1_Q_CS.m

```
# Calculate evolution of the density operator due to
# quadrupole coupling & frequency offset.
  wq=2*pi*vq;
```

```
  wos=2*pi*vos;
# factor=I(I+1)/3, as def. by EBW
# vq=3e^2qQ/(4*h*I(2I-1))
  factor=2/3;
  Id=factor*eye(3);
  Hq=wq*((Iz*Iz)-Id);
  Hcs=wos*Iz;
  dum=i*(Hcs+Hq)*t_evol;
  prop=expm(-dum);
  rho=prop'*rho*prop;
```

decomp_1.m

```
# Decompose the density operator, rho, into single transition
  operators
# & store in the complex vector st(q). For elements q=1-6,
  st(q) are
# Ix(rs), Iy(rs), respectively, in the order (r,s) = (1,2),
  (1,3),(2,3).
# Orthogonalized polarization coefficients (real), q=7,8 are Q
  and Iz.
# Coefficients for Ix and Iy are st(9) and st(10).
  q=0;
  for r=1:1:2;
    for s=r+1:1:3;
      q=q+1;
      st(q)=rho(r,s)+rho(s,r);
      q=q+1;
      st(q)=i*(rho(r,s)-rho(s,r));
    endfor;
  endfor;
  st(7)=(1/6)*trace(Q*rho);
  st(8)=.5*trace(Iz*rho);
  st(9)=.5*trace(Ix*rho);
  st(10)=.5*trace(Iy*rho);
  for j=1:1:10;
    if abs(st(j)) < .00000001;
      st(j)=0;
    endif
  endfor;
```

prepCurve.m

```
# Preparation curve calculation
#vp is the quadrupole coupling constant in Hz & T2 is the
  relaxation time in s
  vp=1800
  wp=2*pi*vp;
  T2=.0022
# t and dt are the initial and increments in time (s) for the
  preparation curve
# npts is the number of time points
  npts=100
  t=.00001e-06
  dt=40e-06
  fac=1
  mfac=exp(-2*dt/T2);
  for j=1:1:npts
    wpt=wp*t;
    u=sqrt(3.*wpt);
# the library function quadgk is used to calculate the
  numerical integrals
# cx2=cos(x^2) and sx2=sin(x^2)
    x=quadgk("cx2",0,u);
    y=quadgk("sx2",0,u);
    I2(j)=.5*(1.-(1/u)*(x*cos(wpt)+y*sin(wpt)))*fac;
    t=t+dt;
    fac=fac*mfac;
  endfor
# print the prep curve to the screen
I2(:)
```

cx2.m

```
function y=cx2(x)
  y=cos(x.^2);
endfunction
```

sx2.m

```
function y=sx2(x)
  y=sin(x.^2);
endfunction
```

References

[1] T. Meersmann, S.A. Smith, G. Bodenhausen, Multiple-quantum filtered xenon-131 NMR as a surface probe, Phys. Rev. Lett. 80 (1998) 1398–1401.
[2] Y. Sharf, Y. Seo, U. Eliav, S. Akselrod, G. Navon, Mapping strain exerted on blood vessel walls using deuterium double-quantum-filtered MRI, Proc. Nat. Acad. Sci. U.S.A. 95 (1998) 4108–4112.
[3] C. Sun, G.S. Boutis, Investigation of the dynamical properties of water in elastin by deuterium Double Quantum Filtered NMR, J. Magn. Reson. 205 (2010) 86–92.
[4] L. Frish, N. Friedman, M. Sheves, Y. Cohen, The interaction of water molecules with purple membrane suspension using H-2 double-quantum filter, H-1 and H-2 diffusion nuclear magnetic resonance, Biopolymers 75 (2004) 46–59.
[5] U. Eliav, M. Komlosh, P.J. Basser, G. Navon, Characterization and mapping of dipolar interactions within macromolecules in tissues using a combination of DQF, MT and UTE MRI, NMR Biomed. 25 (2012) 1152–1159.
[6] G. Navon, U. Eliav, D.E. Demo, B. Blumich, Study of order and dynamic processes in tendon by NMR and MRI, J. Magn. Reson. Imaging 25 (2007) 362–380.
[7] R. Fechete, D.E. Demco, B. Blumich, Parameter maps of H-1 residual dipolar couplings in tendon under mechanical load, J. Magn. Reson. 165 (2003) 9–17.
[8] T. Meersmann, M. Deschamps, G. Bodenhausen, Probing aerogels by multiple quantum filtered Xe-131 NMR spectroscopy, J. Am. Chem. Soc. 123 (2001) 941–945.
[9] M. Rance, O.W. Sorensen, W. Leupin, H. Kogler, K. Wuthrich, R.R. Ernst, Uniform excitation of multiple-quantum coherence – application to 2-dimensional double-quantum spectroscopy, J. Magn. Reson. 61 (1985) 67–80.
[10] A. Wokaun, R.R. Ernst, Selective excitation and detection in multilevel spin systems – application of single transition operators, J. Chem. Phys. 67 (1977) 1752–1758.
[11] R.J. Wittebort, Selective excitation and quadrupole connectivities in deuterium NMR of paramagnetic solids, J. Magn. Reson. 83 (1989) 626–629.
[12] M. Deschamps, I. Burghardt, C. Derouet, G. Bodenhausen, D. Belkic, Nuclear magnetic resonance study of xenon-131 interacting with surfaces: effective Liouvillian and spectral analysis, J. Chem. Phys. 113 (2000) 1630–1640.
[13] R.R. Ernst, G. Bodenhausen, A. Wokaun, Principles of Nuclear Magnetic Resonance in One and Two Dimensions, Oxford University Press, New York, Oxford, 1989.
[14] R.J. Wittebort, E.T. Olejniczak, R.G. Griffin, Analysis of deuterium nuclear-magnetic-resonance line-shapes in anisotropic media, J. Chem. Phys. 86 (1987) 5411–5420.
[15] R. Fechete, D.E. Demco, B. Blumich, Order parameters of the orientation distribution of collagen fibers in Achilles tendon by H-1 NMR of multipolar spin states, NMR Biomed. 16 (2003) 479–483.
[16] G. Bodenhausen, R.L. Vold, R.R. Vold, Multiple quantum spin-echo spectroscopy, J. Magn. Reson. 37 (1980) 93–106.
[17] G. Drobny, A. Pines, S. Sinton, W.S. Warren, D.P. Weitekamp, Selectivity in multiple-quantum spectroscopy, Philos. Trans. Roy. Soc. A – Math. Phys. Eng. Sci. 299 (1981) 585–592.
[18] S. Vega, T.W. Shattuck, A. Pines, Fourier-transform double-quantum NMR in solids, Phys. Rev. Lett. 37 (1976) 43–46.
[19] G. Bodenhausen, H. Kogler, R.R. Ernst, Selection of coherence-transfer pathways in NMR pulse experiments, J. Magn. Reson. 58 (1984) 370–388.
[20] William H. Press, Brian P. Flannery, Saul A. Teukolsky, William T. Vetterling, Numerical Recipes in C: The Art of Scientific Computing, Cambridge University Press, 40 West St., New York, New York, 1988.
[21] T.M. Barbara, R. Tycko, D.P. Weitekamp, Composite sequences for efficient double-quantum excitation over a range of spin coupling strengths, J. Magn. Reson. 62 (1985) 54–64.
[22] B.C. Starcher, M.J. Galione, Purification and comparison of elastins from different animal species, Anal. Biochem. 74 (1976) 441–447.
[23] Q.W. Zhang, H.M. Zhang, K.V. Lakshmi, D.K. Lee, C.H. Bradley, R.J. Wittebort, Double and triple resonance circuits for high-frequency probes, J. Magn. Reson. 132 (1998) 167–171.